

Brittle-to-ductile transition and strain relaxation in $\text{Si}_{1-x}\text{Ge}_x$ linearly graded buffers

Riccardo Civiero,¹ Elena Campagna,² Afonso Cerdeira Oliveira,¹ Marvin Hartwig Zoellner,³
Davide Impelluso,¹ Daniel Chrastina,¹ Giovanni Capellini,^{2,3} and Giovanni Isella¹

¹*LNESS Dipartimento di Fisica, Politecnico di Milano,
via F. Anzani 42, 22100 Como, Italy.*

²*Dipartimento di Scienze, Università degli Studi Roma Tre,
Viale G. Marconi 446, Roma 00146, Italy*

³*IHP - Leibniz Institute for High Performance
Microelectronics, Frankfurt (Oder) 15236, Germany*

(Dated: December 23, 2025)

arXiv:2512.19121v1 [cond-mat.mtrl-sci] 22 Dec 2025

Abstract

The strain-relaxation mechanism of a set of $\text{Si}_{0.6}\text{Ge}_{0.4}$ linearly graded buffers (LGBs), grown following different temperature profiles, has been investigated by means of defect-etching and variable-temperature high-resolution X-ray diffraction (VT-HR-XRD). Defect-etching experiments demonstrate that a sharp increase of threading dislocation density (TDD) from $3 \times 10^5 \text{ cm}^{-2}$ to $1.2 \times 10^6 \text{ cm}^{-2}$ takes place when the final growth temperature exceeds a critical value $T_c \approx 530^\circ\text{C}$. VT-HR-XRD measurements show that in low TDD samples extra relaxation takes place for annealing temperatures larger than T_c , thanks to the nucleation of new dislocations. These results indicate that, below T_c , strain relaxation is driven by the gliding of existing dislocations while above T_c new dislocations are nucleated, suggesting a link with our results and the brittle-to-ductile transition in $\text{Si}_{1-x}\text{Ge}_x$ alloys.

I. INTRODUCTION

Strain-relaxed buffer-layers (SRBs) play a key-role in hetero-epitaxy, enabling the deposition of strained-engineered active layers on commercially available substrates. An ideal SRB should plastically accommodate the lattice mismatch between substrate and active layer, through the introduction of misfit dislocations (MDs), yet minimizing the density of threading dislocations (TDs) which degrades the electro-optical properties of the device layer [1].

In constant composition SRBs, misfit segments accumulate at the buffer/substrate interface, hindering the glide of existing dislocations and promoting the nucleation of new dislocations. As a result, in the $\text{Si}_{1-x}\text{Ge}_x/\text{Si}$ system, constant composition layers features a TD density (TDD) exceeding 10^7 cm^{-2} already for $x \approx 0.3$ and monotonically increasing with Ge content [2].

More than 40 years ago Abrahams *et. al.* introduced linearly graded buffers (LGBs) in $\text{GaAs}_{1-x}\text{P}_x/\text{GaAs}$ hetero-epitaxy with the aim of reducing the TDD, as compared to constant composition buffers [3]. Later, LGBs were extensively used in the early days of strained-Si/ $\text{Si}_{1-x}\text{Ge}_x$ technology [4] before being outperformed by local-stressor approaches [5], however, they recently attracted renewed interest in the framework of semiconductor-based spin qubits [6–8] and integrated photonics in the near and mid infrared [9–11].

In $\text{Si}_{1-x}\text{Ge}_x$ LGBs the alloy composition x is linearly increased from $x = 0$ to the final

target composition x_f and then terminated by a constant composition $\text{Si}_{1-x_f}\text{Ge}_{x_f}$ layer. This approach offers several advantages when compared to constant composition SRBs. Misfit dislocations are not accumulated at the interface, but distributed throughout the linearly graded region, strongly reducing dislocation pinning. In addition, the formation of misfit segments can take place through the gliding of existing TDs avoiding the nucleation of new dislocations. This led Abrahams *et. al.* to predict the existence of a minimal TDD capable of relaxing LGBs independently of the final composition. Yet, extensive work carried out on $\text{Si}_{1-x}\text{Ge}_x$ by Fitzgerald and coworkers [12, 13] showed that LGBs grown by chemical vapor deposition (CVD) features a TDD increase with increasing Ge content, highlighting the role played by processes other than glide, such as nucleation and multiplication, in the relaxation process [14].

Two different trends are expected for the temperature dependence of TDD in glide-driven or nucleation-driven relaxation [14]. As T increases, dislocation glide becomes more effective requiring a comparatively low TDD to promote strain relaxation. In contrast, in nucleation-driven relaxation, a higher T favors the nucleation of more dislocations and an increased TDD.

Most of the experimental works reported so far on $\text{Si}_{1-x}\text{Ge}_x$ LGBs with $x_f \leq 0.5$ are focused on epilayers deposited by CVD in the 650-1000°C temperature range [12, 15, 16]. With the aim of studying the competition between glide and nucleation driven relaxation in a so far unexplored temperature range, we have investigated by means of T-dependent high-resolution X-Ray diffraction (T-HR-XRD), atomic force microscopy (AFM), and etch-pit counting (EPC), a set of $\text{Si}_{1-x}\text{Ge}_x$ LGBs with $x_f = 0.4$ grown at different final temperatures comprised between 510 and 580°C. Interestingly, the switch from glide-driven to nucleation-driven relaxation takes place in a narrow temperature range around $T_c \approx 530^\circ\text{C}$. The analysis of additional LGBs with $x = 0.1, 0.2, 0.3$ confirms the dominance of glide-driven relaxation for samples grown at lower temperatures.

II. EPITAXIAL GROWTH AND CHARACTERIZATION

All samples analyzed in this work were deposited on 100 mm Si(001) wafers by low-energy plasma-enhanced CVD [17] (LEPECVD) using SiH_4 and GeH_4 precursors. In LEPECVD the activation of process gases is performed by means of a discharge plasma [18], whose density

Table I: List of the samples grown for this work, reporting: the sample label, the nominal final Ge content and that experimentally measured by X-ray diffraction, the final growth temperature, the degree of relaxation and surface roughness.

| Sample | Nom. x_f | Meas. x_f | T_f | Relax. | Rough. |
|--------|------------|-------------|-------|--------|--------|
| | (%) | (%) | (°C) | (%) | (nm) |
| A1 | 40 | 39.8 | 510 | 96.9 | 3.12 |
| A2 | 40 | 40.1 | 520 | 97.3 | 2.76 |
| A3 | 40 | 39.9 | 530 | 98.6 | 2.65 |
| A4 | 40 | 39.9 | 550 | 99.3 | 2.52 |
| A5 | 40 | 39.8 | 580 | 100.2 | 2.25 |
| B1 | 30 | 29.5 | 580 | 97.9 | 1.78 |
| B5 | 30 | 29.8 | 627 | 100.1 | 1.21 |
| C1 | 20 | 19.6 | 650 | 98.7 | 1.24 |
| C5 | 20 | 19.8 | 673 | 100.5 | 1.11 |
| D | 10 | 9.8 | 720 | 102.2 | 1.67 |

can be tuned to vary the deposition rate between 0.5 \AA/s and 10 nm/s , independently on the substrate temperature. In this work an average deposition rate of $\approx 8 \text{ nm/s}$ was used. The linear compositional profile was approximated by increasing the Ge concentration in the epilayer in 0.5% steps, [19] to obtain a $7\%/\mu\text{m}$ grading rate. The growth was terminated by a $2 \mu\text{m}$ thick constant composition layer. The samples analyzed in this work are listed in Tab. I.

A first set of $\text{Si}_{1-x}\text{Ge}_x$ LGBs with a final Ge content $x_f = 0.4$, labeled A1 to A5, was grown keeping the substrate temperature at $T=720^\circ\text{C}$ until a Ge content $x = 0.1$ was reached. Subsequently, T was linearly decreased reaching a different final temperature T_f for each one of the samples under consideration, as shown in Fig. 1. At a first glance, a set of isothermally grown epilayers might seem a better choice for the study of T -dependent relaxation mechanism. Yet, in Si and Ge diffusion coefficients, vacancy concentrations [20] and dislocation velocity [21] linearly scale with the respective melting points, making the physical mechanism relevant at a given temperature quite different in Si-rich or Ge-rich alloys. A temperature profile decreasing with the Ge content x should, instead, provide a

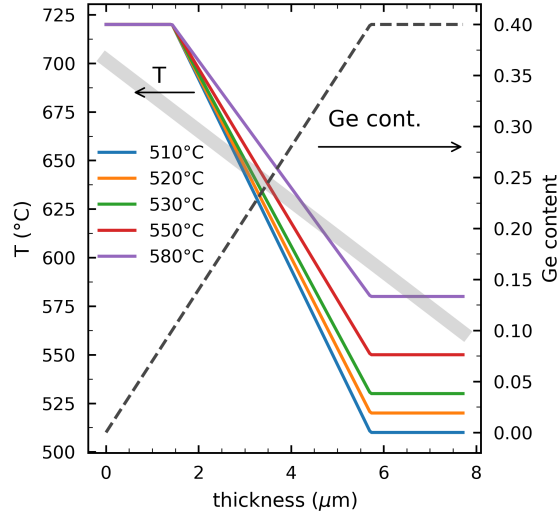


Figure 1: Variation of temperature (left axis) and composition (right axis) during growth for the set of LGBs featuring $x_f = 0.4$ and different final temperatures. The gray area shows an estimation the brittle -ductile transition temperature in $\text{Si}_{1-x}\text{Ge}_x$.

similar energy landscape throughout the LGB growth. In addition, the employed variable-temperature growth protocol kinetically suppress surface roughening, which might impact dislocation nucleation and glide, [13] without the need of chemical-mechanical polishing steps commonly employed in thermal-CVD grown LGBs.

LGBs with $x_f = 0.3$ (B1 and B5), $x_f = 0.2$ (C1 and C5) and $x_f = 0.1$ (D) were also deposited. The T profile of samples B1 (B5) overlaps that of sample A1 (A5) in the common compositional range (*i. e.* $x \leq 0.3$). In the same way samples C1 and C5 share the same T profile of A1 and A5 for $x \leq 0.2$. In short, samples B and C can be considered as “snapshots” of the corresponding A-samples at intermediate points ($x = 0.3, 0.2$) of the growth. The series is completed by a LGB with $x_f = 0.1$ deposited at a constant $T=720^\circ\text{C}$.

A Rigaku SmartLab diffractometer, equipped with a DHS1100 oven from Anton Paar was used for temperature variable high-resolution X-ray diffraction (VT-HR-XRD) measurements [22] performed in N_2 atmosphere to avoid surface oxidation. The residual in-plane strain ϵ_{\parallel} and final Ge content x_f of the LGBs were determined using reciprocal space maps (RSMs) of the (004) and steep-incidence (224) reflections. The degree of relaxation $\beta = 1 - \epsilon_{\parallel}/f$ was obtained by calculating the lattice mismatch f , between the $\text{Si}_{1-x_f}\text{Ge}_{x_f}$ top layer and the Si substrate, using the quadratic interpolation of the $\text{Si}_{1-x}\text{Ge}_x$ lattice parameter reported in

Ref. [23].

Defect etching was carried out using two different etching solutions: the Secco etch and the cold Schimmel etch [24]. Etch-pit counting was performed using differential interference contrast (DIC) optical microscopy averaging over 10 field-of-view each one covering a $260 \mu\text{m} \times 120 \mu\text{m}$ region. Atomic force microscopy (AFM) was employed to determine the root mean square (RMS) roughness of the sample surface, averaging over ten $20 \mu\text{m} \times 20 \mu\text{m}$ scans.

III. RESULTS AND DISCUSSION

The Ge content x_f and degree of relaxation, obtained from RSMs similar to that shown in Fig. 2a), are reported in Tab. I. It can be noticed that the measured Ge content matches, within the experimental error, the targeted x_f , independently on the T-profile employed for the deposition. The degree of relaxation is, instead, affected by the growth temperature, with samples grown at higher temperatures being more relaxed. Over relaxation is observed for samples A5, B5, C5 and D, indicating that tensile-strain, originating from the thermal mismatch between Ge and Si, contributes to the measured room-temperature residual strain [22].

All $\text{Si}_{0.6}\text{Ge}_{0.4}$ LGBs are characterized by a cross-hatch pattern similar to that shown in Fig. 2b, with an RMS-roughness decreasing with temperature from 3.12 nm to 2.25 nm.

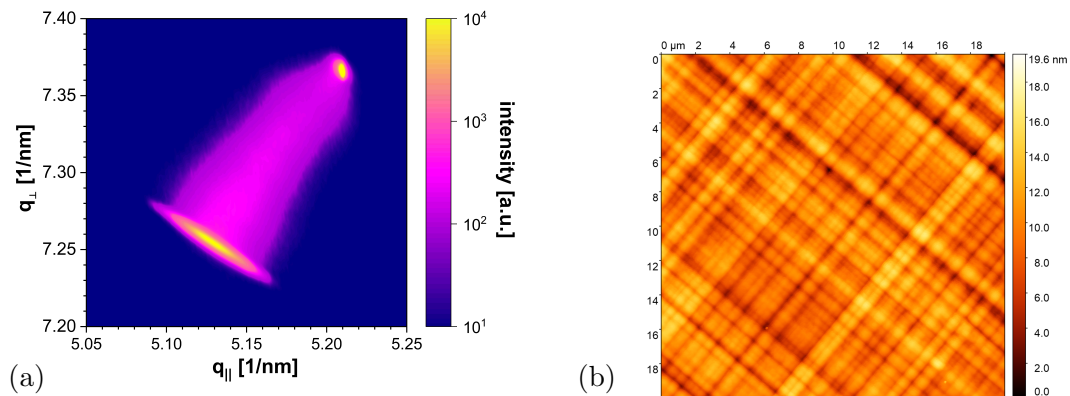


Figure 2: Structural characterization of sample A5. a) Room temperature RSM around the (224) diffraction peak showing the continuous variation of composition between the Si substrate and the $\text{Si}_{0.6}\text{Ge}_{0.4}$ relaxed buffer. b) AFM image of the cross-hatch pattern.

In previous literature reports [13], a direct correlation between roughness and TDD was observed in thermal-CVD samples where, however, the RMS roughness typically exceeds 100 nm. In our case, the RMS roughness is relatively low in all samples and, as shown in Fig. 3, features a trend opposite to that of measured TDD, ruling out a possible impact of surface roughness on plastic-relaxation.

Etch-pit counting results for the $\text{Si}_{0.6}\text{Ge}_{0.4}$ series (samples A1-5 in Tab.I) are shown in Fig. 3a. It can be noticed that: (a) the TDD sharply increases from $\sim 3 \times 10^5 \text{ cm}^{-2}$ to $\sim 1.2 \times 10^6 \text{ cm}^{-2}$ varying T_f from 520 to 530°C; (b) Low-T samples (A1 and A2) do not feature any statistically relevant density of dislocation pile-ups which, instead, contribute substantially to the total TDD in high-T samples (A3 to A5).

The as-grown $\text{Si}_{0.6}\text{Ge}_{0.4}$ LGBs were analyzed by means of VT-HRHRD from $T=27^\circ\text{C}$ to $T=557^\circ\text{C}$ in 50°C steps. The degree of relaxation, measured at every step is indicated by the empty circles in Fig. 4. Subsequently the samples were cooled down re-measuring the

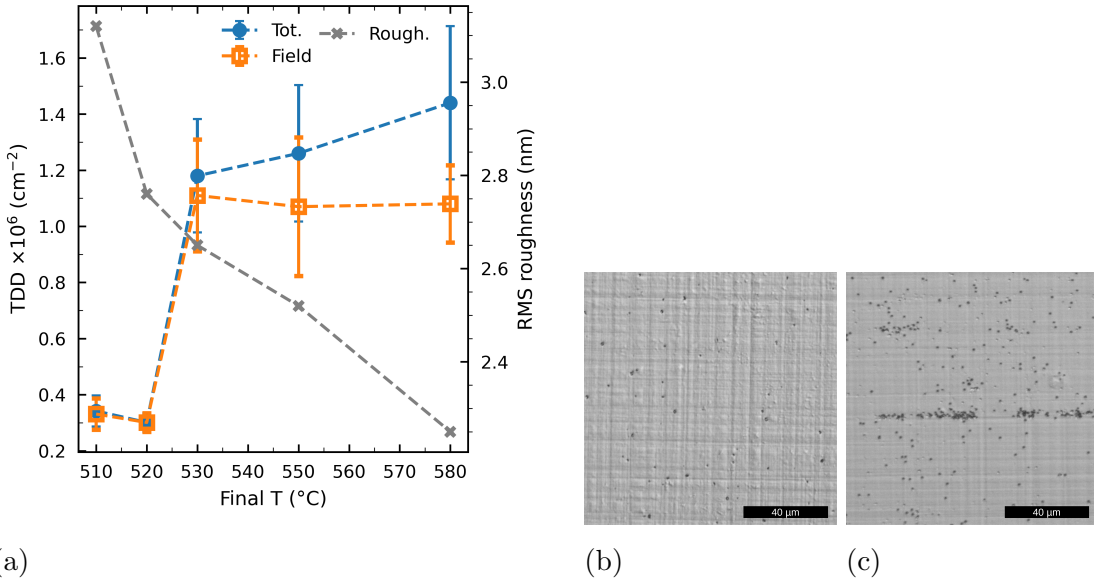


Figure 3: Threading dislocation density in $\text{Si}_{0.6}\text{Ge}_{0.4}$ LGBs. (a) TDD *vs.* final temperature. The plot reports the density of so-called field TDs, *i.e.* dislocations not piled-up in clusters, and the total number of TDs. The roughness dependence on the final temperature can be read on the right-hand *y*-axis. Panels (b) and (c) show representative optical micro-graphs obtained after defect etching of samples A1 ($T_f = 510^\circ\text{C}$) and A5 ($T_f = 580^\circ\text{C}$), respectively.

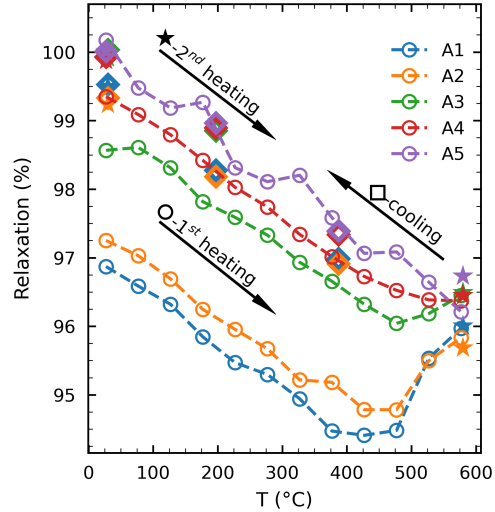


Figure 4: Degree of relaxation at different post-growth annealing temperatures as measured by VT-HRHRD. For each of the A-samples ($x_f = 0.4$) listed in Tab. I the relaxation has been measured during a 1st heating ramp (empty circles), cool-down (empty diamonds) and a 2nd heating ramp and cool-down (stars)

degree of relaxation at $T = 387, 197$ and 27°C (empty-diamonds in Fig. 4). Eventually the samples were heated again at $T = 557^\circ\text{C}$ and cooled down at $T = 27^\circ\text{C}$ (filled stars in Fig. 4). It can be noticed that, during the first heating cycle, the degree of relaxation decreases for all samples up to $T \approx 500^\circ\text{C}$. As T increases, the (tensile) thermal-strain, accumulated during cool-down after the deposition, is progressively reduced, unveiling the residual (compressive) mismatch-strain, which, not surprisingly, is larger for samples deposited at an average lower- T .

For $T \gtrsim 500^\circ\text{C}$ two distinct behaviors are observed for samples A1-A3 and A4-A5, respectively. In samples A4 and A5 the relaxation measured during the different heating and cooling cycles reversibly follows the same path, indicating that plastic relaxation has reached the equilibrium value achievable for $T = 577^\circ\text{C}$ in the case of $\text{Si}_{0.6}\text{Ge}_{0.4}$ LGBs deposited following the $T_f = 580^\circ\text{C}$ and $T_f = 550^\circ\text{C}$ temperature profile. For these samples the T -dependent degree of relaxation can be attributed solely to the elastic, thermal-induced strain.

The relaxation of samples A1-A3 is, instead, characterized by a clear step taking place between $T \approx 500^\circ\text{C}$ and $T \approx 550^\circ\text{C}$, showing that an additional relaxation of misfit-strain is obtained when annealing these samples above their final deposition temperature $T_f = 510^\circ\text{C}$,

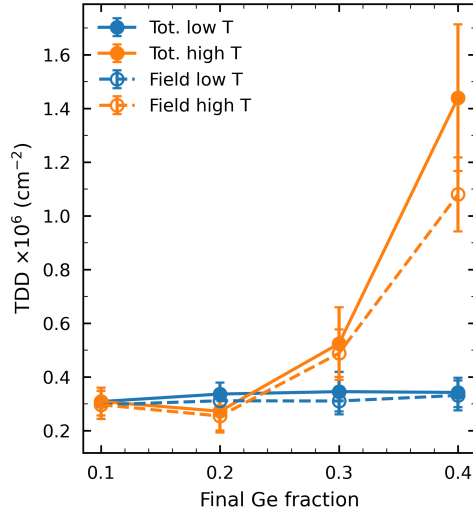


Figure 5: Total (filled circles) and field (empty circles) density of TDs in $\text{Si}_{1-x}\text{Ge}_x$ LGBs with increasing Ge content. The low T data-points refer to samples A1, B1, C1, and D, the high T data-points to A5, B5, and C5 described in Tab. I.

$T_f = 520^\circ\text{C}$ and $T_f = 530^\circ\text{C}$, respectively. Such extra-relaxation is clearly plastic, as indicated by the non-reversible relaxation path followed during cool-down. The second annealing step confirms that a stable configuration, although at slightly different relaxation levels, has been reached for all samples after the first annealing cycle.

In summary the increase of TDs for $T \sim 520\text{-}530^\circ\text{C}$ (see Fig. 3) is mirrored by a sudden increase of plastic relaxation observed by VT-HRXRD in a similar temperature range as detailed in Fig. 4. Etch-pit counting performed on the annealed samples yields TDD in the $1 - 3 \times 10^6 \text{ cm}^{-2}$ range for all samples, demonstrating that, during post-growth annealing, the extra relaxation takes place mainly by the nucleation of new dislocation and not by gliding of existing TDs. The etch-pit counting and VT-HRXRD measurements consistently support the idea that, after the initial phase of the deposition where dislocation are nucleated in both the low-T (A1) and high-T (A5) samples two different relaxation mechanisms take place: in A1 the relaxation proceeds mainly by gliding of existing TD, while in A5 new dislocations are nucleated. To confirm this picture the TDD and degree of relaxation of samples with lower Ge content (B, C and D in Tab. I) have also been investigated.

Figure 5 shows the etch-pit counting for the low-T (A1, B1, C1 and D) and high-T (A5, B5, C5, D) $\text{Si}_{1-x}\text{Ge}_x$ LGBs series with $x_f = 0.4, 0.3, 0.2, 0.1$. It can be noticed that, for the

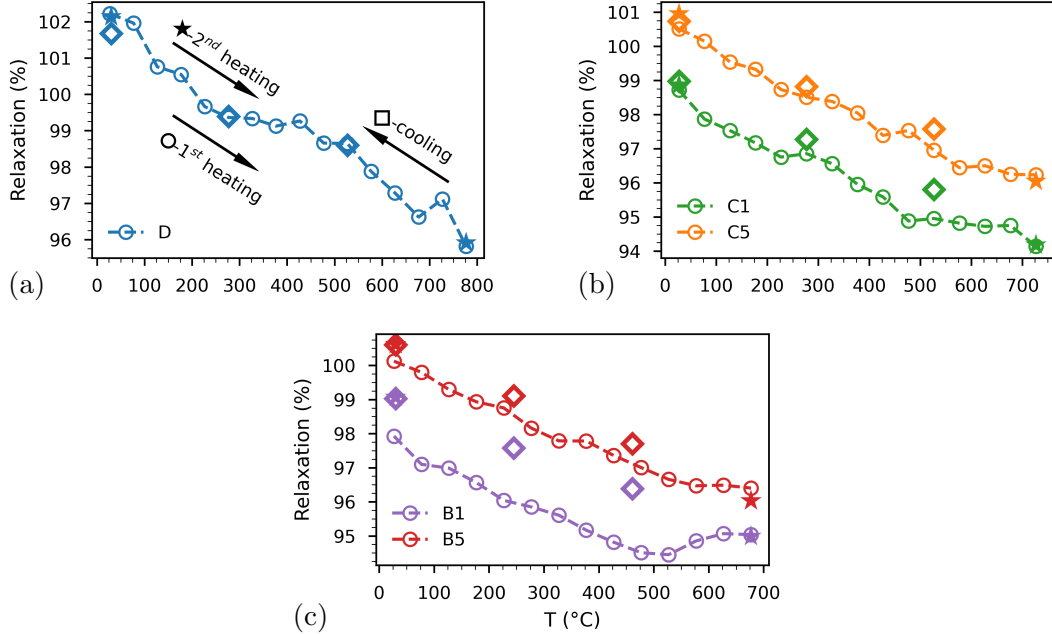


Figure 6: Degree of relaxation at different annealing temperatures for Si_{1-x}Ge_x LGBs with increasing Ge content. Relaxation of (a) sample D measured in the temperature range T=27-777°C (b) samples C1 and C2 for T=27-727°C and (c) B1 and B5 for T=27-677°C.

high-T series the TDD increases for $x_f \gtrsim 0.3$ with an increased contribution from piled-up dislocations. In the low-T case the TDD is, instead, constant in the $x_f = 0.1 - 0.4$ range in agreement with what expected for glide-driven relaxation [3].

VT-HRXRD data reported in Fig.6 confirm that for samples D ($x = 0.1$), C5 and C1 ($x = 0.2$) no sizable change in the plastic relaxation of the misfit strain takes place, upon annealing. On the other hand, a comparison between the VT-HRXRD data of samples B1 ($x = 0.3$ and $T_f=580^\circ\text{C}$) and B5 ($x = 0.3$ and $T_f=627^\circ\text{C}$) shows that additional plastic relaxation, although less pronounced than in the case of sample A1, takes place in B1 for $T \gtrsim 500^\circ\text{C}$.

The relatively narrow temperature range, where the transition from glide- to nucleation-driven relaxation occurs, suggests a possible correlation between our observations and the brittle to ductile transition (BDT) extensively studied in Si [25, 26] and Ge [27] by means of fracture tests performed on indented samples. These studies highlighted a remarkable correlation between the BDT temperature T_c , above which several dislocations are nucleated at the indented crack tip, and the activation energy for dislocation glide U . For a wide range

of materials [28] $U/k_B T_c \sim 25$. Taking the approximate values of 1.5 and 2 eV for U in Ge and Si [28], the T_c of the two materials can be linearly interpolated to obtain a rough estimation of the BDT temperature of $\text{Si}_{1-x}\text{Ge}_x$ alloys as shown by the gray region in Fig. 1.

It can be noticed that, during the growth of samples A5, the deposition temperature is always above T_c favoring the nucleation of new dislocations. On the contrary, in the last phases of sample A1 the deposition temperature falls below T_c inhibiting the nucleation of more dislocations and leaving glide as the only active relaxation mechanism. Although the comparison between fracture tests and epitaxial growth must be taken with care, our data might open up new perspective for the study of the role played by the BDT in hetero-epitaxy.

IV. CONCLUSIONS

The relaxation of $\text{Si}_{0.6}\text{Ge}_{0.4}$ LGBs has been investigated in a temperature range hardly accessible by thermal CVD, by growing, thanks to LEPECVD, a set of samples with identical Ge composition but different temperature profiles. Defect-etching and VT-HRHRD indicate that the mechanism driving misfit relaxation switches from the gliding of existing TDs for samples deposited at a final $T \lesssim 520^\circ\text{C}$, to the nucleation of new dislocations for $T \gtrsim 530^\circ\text{C}$. This is confirmed by a set of samples with lower Ge content featuring a composition-independent TDD in the $x = 0.1 - 0.4$ range, a clear signature of glide-driven relaxation. Interestingly, a sharp increase of TDD was previously reported in $\text{Si}_{0.04}\text{Ge}_{0.96}$ LGBs deposited by thermal CVD [14] at $T \geq 550^\circ\text{C}$ suggesting such a behavior to be independent to the specific growth conditions. A tentative explanation of these results can be given in terms of the brittle-to-ductile transition. This opens the way for further studies on such ubiquitous phenomenon, exploiting LGBs as an environment with controlled and tuneable strain-levels.

ACKNOWLEDGMENTS

Part of this work has been carried out within the International Joint Lab “Intelligent Electro-Optical Sensing,” established between IHP - Leibniz Institute for High Performance Microelectronics and the University of Rome Tre. A. C. D. acknowledges the support by the European Union’s Horizon Europe LASTSTEP Project under the grant agreement ID: 101070208. D. I. acknowledges the support by the European Union’s ERC ELECTROPHOT

Project, under the Grant Agreement ID: 101097569.

DATA AVAILABILITY STATEMENT

The data that support the findings of this study are openly available in ZENODO, at <https://zenodo.org/records/17750768>, reference number 17750768.

-
- [1] L. M. Giovane, H.-C. Luan, A. M. Agarwal, and L. C. Kimerling, Correlation between leakage current density and threading dislocation density in SiGe p-i-n diodes grown on relaxed graded buffer layers, *Applied Physics Letters* **78**, 541 (2001).
 - [2] Y. B. Bolkhovityanov, O. P. Pchelyakov, L. V. Sokolov, and S. I. Chikichev, Artificial GeSi substrates for heteroepitaxy: Achievements and problems, *Semiconductors* **37**, 493 (2003).
 - [3] M. S. Abrahams, L. R. Weisberg, C. J. Buiochi, and J. Blanc, Dislocation morphology in graded heterojunctions: GaAs_{1-x}P_x, *Journal of Materials Science* **4**, 223 (1969).
 - [4] F. Schäffler, Strained Si/SiGe heterostructures for device applications, *Solid-State Electronics* **37**, 765 (1994).
 - [5] S. Thompson, M. Armstrong, C. Auth, M. Alavi, M. Buehler, R. Chau, S. Cea, T. Ghani, G. Glass, T. Hoffman, C.-H. Jan, C. Kenyon, J. Klaus, K. Kuhn, Zhiyong Ma, B. McIntyre, K. Mistry, A. Murthy, B. Obradovic, R. Nagisetty, Phi Nguyen, S. Sivakumar, R. Shaheed, L. Shifren, B. Tufts, S. Tyagi, M. Bohr, and Y. El-Mansy, A 90-nm logic technology featuring strained-silicon, *IEEE Transactions on Electron Devices* **51**, 1790 (2004).
 - [6] S. Neyens, O. K. Zietz, T. F. Watson, F. Luthi, A. Nethwewala, H. C. George, E. Henry, M. Islam, A. J. Wagner, F. Borjans, E. J. Connors, J. Corrigan, M. J. Curry, D. Keith, R. Kotlyar, L. F. Lampert, M. T. Madzik, K. Millard, F. A. Mohiyaddin, S. Pellerano, R. Pillarisetty, M. Ramsey, R. Savytsky, S. Schaal, G. Zheng, J. Ziegler, N. C. Bishop, S. Bojarski, J. Roberts, and J. S. Clarke, Probing single electrons across 300-mm spin qubit wafers, *Nature* **629**, 80 (2024).
 - [7] Y. Shimura, C. Godfrin, A. Hikavy, R. Li, J. Aguilera, G. Katsaros, P. Favia, H. Han, D. Wan, K. De Greve, and R. Loo, Compressively strained epitaxial ge layers for quantum computing applications, *Materials Science in Semiconductor Processing* **174**, 108231 (2024).

- [8] D. Jirovec, A. Hofmann, A. Ballabio, P. M. Mutter, G. Tavani, M. Botifoll, A. Crippa, J. Kukucka, O. Sagi, F. Martins, J. Saez-Mollejo, I. Prieto, M. Borovkov, J. Arbiol, D. Chrastina, G. Isella, and G. Katsaros, A singlet-triplet hole spin qubit in planar Ge, *Nature Materials* **20**, 1106 (2021), arXiv: 2011.13755 Publisher: Springer US.
- [9] D. Marris-Morini, V. Vakarín, J. M. Ramírez, Q. Liu, A. Ballabio, J. Frigerio, M. Montesinos, C. Alonso-Ramos, X. Le Roux, S. Serna, D. Benedikovic, D. Chrastina, L. Vivien, and G. Isella, Germanium-based integrated photonics from near- to mid-infrared applications, *Nanophotonics* **7**, 1781 (2018), iSBN: 0000000213.
- [10] V. Vakarín, J. M. Ramírez, J. Frigerio, A. Ballabio, X. Le Roux, Q. Liu, D. Bouville, L. Vivien, G. Isella, and D. Marris-Morini, Ultra-wideband ge-rich silicon germanium integrated mach-zehnder interferometer for mid-infrared spectroscopy, *Optics Letters* **42**, 3482 – 3485 (2017), cited by: 42; All Open Access, Green Open Access.
- [11] J. Frigerio, C. Ciano, J. Kuttruff, A. Mancini, A. Ballabio, D. Chrastina, V. Falcone, M. De Seta, L. Baldassarre, J. Allerbeck, D. Brida, L. Zeng, E. Olsson, M. Virgilio, and M. Ortolani, Second harmonic generation in germanium quantum wells for nonlinear silicon photonics (2021), cited by: 13; All Open Access, Green Open Access.
- [12] E. Fitzgerald, A. Kim, M. Currie, T. Langdo, G. Taraschi, and M. Bulsara, Dislocation dynamics in relaxed graded composition semiconductors, *Materials Science and Engineering: B* **67**, 53 (1999), iSBN: 0921-5107.
- [13] S. B. Samavedam and E. A. Fitzgerald, Novel dislocation structure and surface morphology effects in relaxed Ge/Si-Ge(graded)/Si structures, *Journal of Applied Physics* **81**, 3108 (1997).
- [14] D. M. Isaacson, C. L. Dohrman, and E. A. Fitzgerald, Deviations from ideal nucleation-limited relaxation in high-Ge content compositionally graded SiGe/Si, *Journal of Vacuum Science & Technology B: Microelectronics and Nanometer Structures Processing, Measurement, and Phenomena* **24**, 2741 (2006).
- [15] Y. Bogumilowicz, J. M. Hartmann, C. Di Nardo, P. Holliger, A.-M. Papon, G. Rolland, and T. Billon, High-temperature growth of very high germanium content SiGe virtual substrates, *Journal of Crystal Growth* **290**, 523 (2006).
- [16] M. H. Zoellner, M.-I. Richard, G. A. Chahine, P. Zaumseil, C. Reich, G. Capellini, F. Montalenti, A. Marzegalli, Y.-H. Xie, T. U. Schüllli, M. Häberlen, P. Storck, and T. Schroeder, Imaging structure and composition homogeneity of 300 mm size virtual substrates for ad-

- vanced cmos applications by scanning x-ray diffraction microscopy, *ACS Applied Materials & Interfaces* **7**, 9031 (2015).
- [17] C. Rosenblad, H. R. Deller, A. Dommann, T. Meyer, P. Schroeter, and H. von Känel, Silicon epitaxy by low-energy plasma enhanced chemical vapor deposition, *J. Vac. Sci. Technol. A* **16**, 2785 (1998).
- [18] M. Rondanini, C. Cavallotti, D. Ricci, D. Chrastina, G. Isella, T. Moiseev, and H. von Känel, An experimental and theoretical investigation of a magnetically confined dc plasma discharge, *Journal of Applied Physics* **104**, 013304 (2008).
- [19] F. Sánchez-Almazán, E. Napolitani, A. Carnera, A. V. Drigo, M. Berti, J. Stangl, Z. Zhong, G. Bauer, G. Isella, and H. Von Känel, Ge quantification of high Ge content relaxed buffer layers by RBS and SIMS, *Nuclear Instruments and Methods in Physics Research, Section B: Beam Interactions with Materials and Atoms* **226**, 301 (2004).
- [20] J. Vanhellefont and E. Simoen, Brother Silicon, Sister Germanium, *Journal of The Electrochemical Society* **154**, H572 (2007).
- [21] A. R. Chaudhuri, J. R. Patel, and L. G. Rubin, Velocities and Densities of Dislocations in Germanium and Other Semiconductor Crystals, *Journal of Applied Physics* **33**, 2736 (1962).
- [22] G. Capellini, M. De Seta, P. Zaumseil, G. Kozlowski, and T. Schroeder, High temperature x ray diffraction measurements on Ge/Si(001) heterostructures: A study on the residual tensile strain, *Journal of Applied Physics* **111**, 073518 (2012).
- [23] J. P. Dismukes, L. Ekstrom, and R. J. Paff, Lattice parameter and density in germanium-silicon alloys 1, **68**, 3021.
- [24] S. Marchionna, A. Virtuani, M. Acciarri, G. Isella, and H. von Kaenel, Defect imaging of SiGe strain relaxed buffers grown by LEPECVD, *Materials Science in Semiconductor Processing* **9**, 802 (2006).
- [25] J. Samuels and S. G. Roberts, The brittle-ductile transition in silicon. I. Experiments, *Proceedings of the Royal Society of London. A. Mathematical and Physical Sciences* **421**, 1 (1989).
- [26] P. B. Hirsch, S. G. R. , and J. Samuels, The brittle-ductile transition in silicon. II. Interpretation, *Proceedings of the Royal Society of London. A. Mathematical and Physical Sciences* **421**, 25 (1989).
- [27] F. Serbena and S. Roberts, The brittle-to-ductile transition in germanium, *Acta Metallurgica et Materialia* **42**, 2505 (1994).

- [28] P. Hirsch and S. Roberts, Comment on the brittle-to-ductile transition: A cooperative dislocation generation instability; dislocation dynamics and the strain-rate dependence of the transition temperature, *Acta Materialia* **44**, 2361 (1996).